Applied Catalysis B: Environmental 240 (2019) 270–276

Contents lists available at ScienceDirect

Applied Catalysis B: Environmental

journal homepage: www.elsevier.com/locate/apcatb

Synergistic effect of the rearranged sulfur vacancies and sulfur interstitials for 13-fold enhanced photocatalytic H_2 production over defective $Zn_2In_2S_5$ nanosheets

Xiao Li, Yao Cheng, Qingping Wu*, Ju Xu, Yuansheng Wang*

CAS Key Laboratory of Design and Assembly of Functional Nanostructures, Fujian Institute of Research on the Structure of Matter, Chinese Academy of Sciences; University of Chinese Academy of Sciences, Fuzhou, 350002, P. R. China

ARTICLE INFO

Keywords:
Sulfur vacancies
Sulfur interstitials
Synergistic effect
Water splitting
H_2 production

ABSTRACT

Intrinsic defect engineered semiconductor photocatalysts have been widely investigated for reaching visible light active photocatalytic H_2 production. However, these defects are usually not stably present, thus requires external elements for stabilization. In this paper, we demonstrate a new strategy for significantly enhancing the photocatalytic H_2 conversion efficiency. The strategy is based on synergistic effect of the properly rearranged sulfur interstitials and sulfur vacancies without introducing any external dopants. Toward this, the defective $Zn_2In_2S_5$ nanosheets are successfully synthesized by a simple hydrothermal method. The synergetic contribution of the rearranged sulfur vacancies and sulfur interstitials within the material is strongly supported by that the photogenerated charge-carrier separation efficiency is obviously (~2-fold) enhanced, and the activity for H_2 production at the end of the fourth cycle test is 13-fold more than that of the beginning of the first cycle test. The rearranged positively charged sulfur vacancies and negatively charged sulfur vacancies in-situ form defect associates, which possess electric filed. We propose that the electric filed could effectively separate the photogenerated charge-carriers, and the positively charged sulfur vacancies act as trapping centers for splitting H_2O via capturing O atoms into vacancy sites. The trapped O atoms can be subsequently removed by Na_2S sacrificial reagent to reactivate the sulfur vacancies. Internally consistent reaction mechanism is proposed that describe the synergistic contribution of the rearranged sulfur vacancies and sulfur interstitials to the dramatically enhanced activity for photocatalytic H_2 production. This inspires new design of defective semiconductor materials.

1. Introduction

Hydrogen represents ideal clean fuel that possesses excellent energy density (122 kJ/g) without releasing any secondary pollutants during combustion in air [1–3]. Photocatalytic water splitting utilizing visible light (main part of the solar light) has been tremendously investigated for converting energy of light into clean hydrogen [4,5]. However, traditional TiO_2 based semiconductor photocatalysts are mainly suffering from only absorbing UV light or low H_2 conversion efficiency [6,7]. To reach visible light activity, the semiconductor photocatalysts are usually doped with external elements or coupled with other narrow bandgap semiconductors to form heterojunctions [8]. However, the complicated synthetic process for these materials is either expensive or contaminative [9].

Close inspection demonstrates that photocatalytic performance of the materials greatly depends on their optical and electrical properties, which are mainly determined by the intrinsic defects within the materials [10,11]. Intrinsic defect engineered semiconductor photocatalysts have been widely investigated to overcome these disadvantages without introducing any external dopants [12]. Among those, $Zn_mIn_2S_{3+m}$ series materials with layered structures along *c*-axis (commonly hexagonal and rhombohedral structures) have demonstrated much higher photocatalytic H_2 production activity comparing to that of TiO_2 based materials [13,14]. The intrinsic defects within the $Zn_xIn_3S_{x+3}$ include sulfur vacancies, sulfur interstitials, zinc vacancies, zinc interstitials, indium vacancies and indium interstitials [15]. Most commonly investigated intrinsic defects in sulfur metal base materials are positively charged sulfur vacancies [16], which mainly originate from dislocation of the lattice sulfurs [17]. However, dislocation of the lattice sulfurs not only creates positively charged sulfur vacancies, but also produces negatively charged sulfur interstitials. Practical study demonstrates that these positively and negatively charged defects can

* Corresponding authors.
E-mail addresses: qpwu@fjirsm.ac.cn (Q. Wu), yswang@fjirsm.ac.cn (Y. Wang).

https://doi.org/10.1016/j.apcatb.2018.09.008
Received 10 May 2018; Received in revised form 23 July 2018; Accepted 4 September 2018
Available online 05 September 2018

be coexistent within the materials without recombination to form lattice atoms [18]. However, these defects are often randomly distributed (not properly located), and could easily act as photo-generated charge-carrier recombination centers [19], resulting in relatively low H_2 conversion efficiency. Furthermore, the reaction mechanism of these defects for photocatalytic splitting water into H_2 remains unclear [20–22].

Recent report from Guan et al. demonstrates that oppositely charged bismuth vacancies and oxygen vacancies could form stable associates upon assistance of platinum, which improve the photocatalytic degradation of dye over ultrathin bismuth oxychloride Nanosheets [23]. Notably, when the thickness of the materials is reduced to ultrathin nanosheets (only a few layers), a large proportion of interior atoms is exposed on the surface. This would facilitate the dislocation of lattice atoms to form oppositely charged intrinsic defects [24]. In addition, the nanosheet materials would also provide an ideal catalytic model for understanding the contribution of the defects to the photocatalytic performance [25].

However, the synthesized materials (hetero-structure) are very complicated and expensive (requiring Pt). Alternatively, formation of stable intrinsic defect associates without assistance of any external elements would be promising for photocatalytic applications [26]. In contrast, the properly rearranged defects that exactly match the material structure may be stably present and significantly improve the photocatalytic performance without assistance of external elements. This may be achieved through structure rearrangement.

In this paper, we propose a new strategy that dramatically promotes the photocatalytic water splitting for H_2 production. The strategy is based on in-situ rearrangement of positively charged sulfur vacancies and negatively charged sulfur interstitials within $Zn_2In_2S_5$ without introducing any external elements. In this way, the defective $Zn_2In_2S_5$ nanosheets have been successfully synthesized by a hydrothermal method. We show for the first time that the synergetic effect of the rearranged sulfur vacancies and sulfur interstitials significantly enhance the charge-carrier separation efficiency and dramatically promote the water splitting for H_2 production. Series internally consistent reaction equations are proposed that describe the synergistic contribution of the sulfur vacancies and sulfur interstitials for photocatalytic splitting H_2O into H_2.

2. Experimental

2.1. Synthesis of defective $Zn_2In_2S_5$ nanosheets

The defective $Zn_2In_2S_5$ nanosheets were new synthesized by a simple hydrothermal method. All chemical reagents are analytical grade without any further purification before use. Firstly, 30 ml ultrapure water (18.2 MΩ cm) with 30 ml ethanol were homogeneously mixed and filled into a 100 ml Teflon-lined autoclave. Secondly, 1 mmol $Zn(NO_3)_2$, 2 mmol $In(NO_3)_3$ and 8 mmol thioacetamide were added with vigorous stirring to form a homogenous colorless solution. Subsequently, the Teflon was sealed and heated at 180 °C for 24 h. After cooling to room temperature, the obtained claybank products were separated by a centrifuger (10,000 rpm, 3 min), then washed by the distilled water and ethanol. The final powder samples were obtained after continuously drying in air at 60 °C.

2.2. Photocatalytic evaluations

The photocatalytic evaluations were performed in a Pyrex reaction cell connected to a closed gas system. The Pyrex reaction cell was externally circulated with constant temperature (25 °C) water to rule out the impact of the temperature to photocatalytic reactions. Typically, 0.05 g sample powders were directly suspended in 100 ml of aqueous solution containing 0.1 M Na_2S with continuously stirring before reach adsorption-desorption equilibrium. The photocatalytic reactions were carried out under irradiation of a 300 W Xenon lamp (PLS-SXE 300 CUV), which is equipped with a 420 nm cut-off light filter to filter out the UV light. The amount of hydrogen produced was separated by a carbon molecular sieve packed column (TDX-01) and measured by an online gas chromatograph (Shimadzu, GC-2014) through a thermal conductive detector (TCD) using 99.999% argon as carrier gas. After every cycle test, the sample solution was standing for 7 days (light off) before next cycle test.

2.3. Structure characterization

The crystal structure of the samples before and after photocatalytic cycle tests was measured by XRD patterns, recording on a Miniflex 600 diffractometer using Cu-Kα radiation (40 kV, 15 mA). The crystal morphology was recorded by transmission electron microscopy (TEM, JEM-2010). TEM specimens were prepared by ultrasonic dispersion of the sample powders in ethanol to the surface of a carbon-coated copper grid with subsequent drying at room temperature in air for 30 min.

2.4. Defect characterization

The electron paramagnetic resonance (EPR) with a Bruker E500 spectrometer was used for measuring defect species within the materials at room temperature. The photoluminescence (PL) spectra were recorded on a spectrofluorometer (Edinburg Instruments FLS920) using a 450 W Xenon lamp for excitation (excitation wavelength: 365 nm).

2.5. Photoelectrical measurement

The photoelectrochemical measurements were performed in the cell equipped with three electrodes, namely working electrode, counter Pt electrode and reference electrode (Ag/AgCl). The photocurrent tests were carried out under irradiation of a 500 W Xenon lamp (PLS-SXE300C). The UV part of the light was removed using a 420 nm cut-off light filter. For working electrode, 20 mg of sample powders was directly dispersed into the 0.5 ml ethanol with subsequent sonication to form slurry. The conductive tape was applied to adhere to a part of FTO glasses to leave an area of 1×1 cm^2 for depositing 20 µl slurry.

3. Results and discussion

The morphology and crystal structure of the synthesized material is firstly identified by transmission electron microscopy (TEM). As indicated in Fig. 1a, approximate several hundred nanometer transparent sheets are clearly observed. This indicates that the synthesized material is composed of ultra-thin nanosheets. In addition, the selected area electron diffraction (SAED) inserted in Fig. 1a demonstrates a set of clear diffraction rings, which correspond to (015) and (116) lattice planes of rhombohedral $Zn_2In_2S_5$ [27]. The high magnification TEM images show that the synthesized material is composed of irregularly disconnected lattice fringes (Fig. 1b). One of possible explanations to the formation of irregularly disconnected lattice fringes is that the material may naturally contain a certain amount of randomly distributed defects [28], which will be further analyzed later. The other possibility is that the material is partially amorphous. However, the presence of partially amorphous structure is not likely, since the SAED patterns demonstrate a set of clear polycrystalline diffraction rings.

The synthesized defective $Zn_2In_2S_5$ nanosheets are repeatedly evaluated for photocatalytic splitting H_2O into H_2 using Na_2S as sacrificial reagent under visible light irradiation (Fig. 2). While all experimental conditions are kept the same, continuously increased H_2 production rate (activity) is found with increase of irradiation time. Compared to the catalytic performance at the first hour (39 µmol/g/h) of Test 1, more than 3-fold increased activity for H_2 production (145 µmol/g/h) at the end of Test 1 (fifth hour) is obtained. The significantly enhanced activity for H_2 production with increase of irradiation time implies that the material structure may be rearranged and

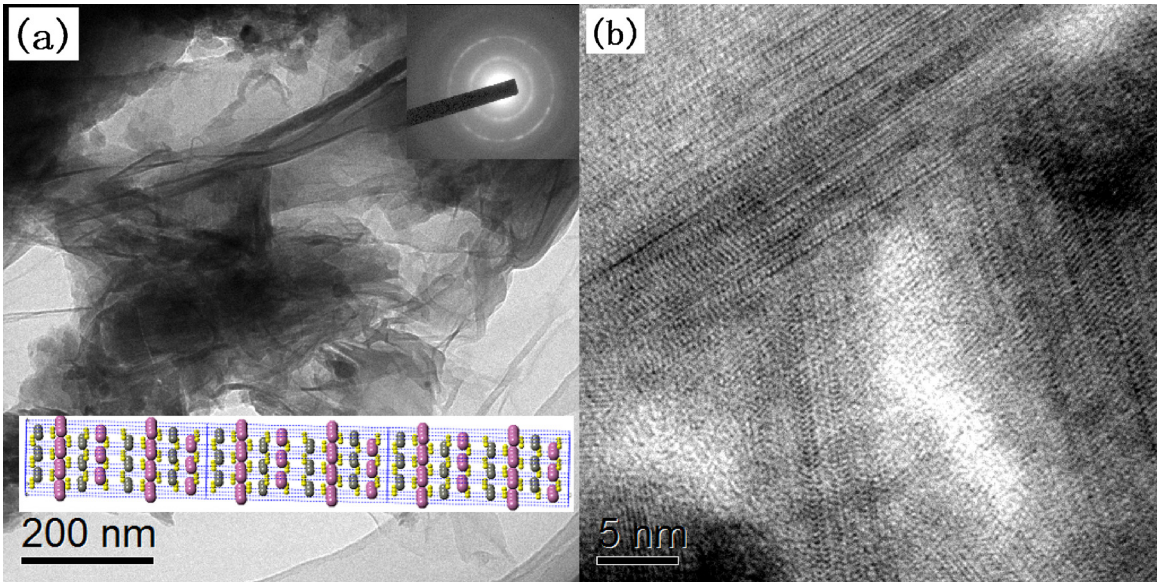

Fig. 1. **(a)** TEM micrograph inserted with selected area electron diffraction (SAED) patterns and rhombohedral $Zn_2In_2S_5$ crystal structure. **(b)** High magnification TEM image of the synthesized material.

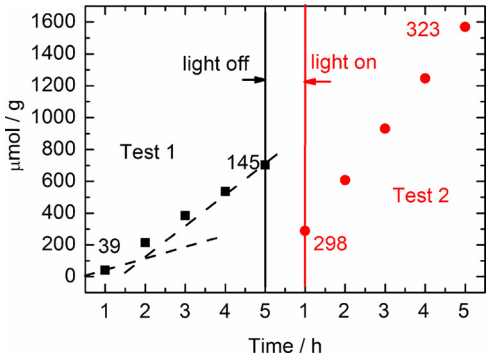

Fig. 2. Photocatalytic cycle tests (Test 1 and Test 2) of defective $Zn_2In_2S_5$ nanosheets for splitting water into H_2 under visible light irradiation using Na_2S as sacrificial reagent.

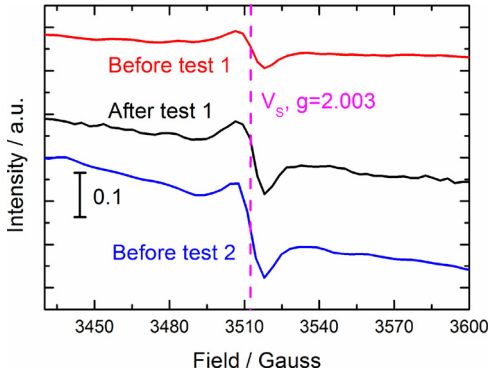

Fig. 3. EPR spectra of the defective $Zn_2In_2S_5$ nanosheets before test 1, after test 1 and before test 2.

optimized during the photocatalytic process. Further support is provided by the repeated test of photocatalytic performance after standing (light off) process. Again, the H_2 production rate (323 μmol/g/h) at the end of Test 2 is much more (~8-fold) than that of the beginning of Test 1. As intrinsic defects (e.g., sulfur vacancies, sulfur interstitials, zinc vacancies) are often naturally present within the metal sulfur based material [29], one of the possible explanations is that the rearrangement of these defects may contribute to the dramatically enhanced activity for H_2 production.

The possible intrinsic defects that present are directly measured by EPR spectra. For the synthesized material (before test 1), no external dopants are introduced, as evidenced by XPS survey spectrum in Fig. S1. Six intrinsic defects (sulfur vacancies, sulfur interstitials, zinc vacancies, zinc interstitials, indium vacancies, indium interstitials) are possibly co-existent within the materials. As shown in Fig. 3, the synthesized $Zn_2In_2S_5$ nanosheets (before test 1) naturally possess a certain amount of sulfur vacancies, as observation of EPR feature signal at g = 2.003 (Fig. 3) [30], while no other vacancies are observed. In contrast, sulfur and zinc interstitials don't possess any unpaired electrons, are therefore not possible to be detected from EPR spectra. However, the coexistence of sulfur interstitials in the synthesized material can be directly observed from photoluminescence (PL) spectra in Fig. S2 with a feature peak at 418 nm [31], whereas the other interstitials (e.g., peak at 423.9 nm for zinc interstitials [31]) are not present. The co-existence of the sulfur vacancies with sulfur interstitials in the synthesized material could be due to dislocation of the lattice sulfurs [32] ($S_S^X \rightarrow V_S^{\bullet\bullet} + S_i^{//}$, written using standard Kröger-Vink notation [33], while $V_S^{\bullet\bullet}$ and $S_i^{//}$ represent divalent positively charged sulfur vacancy and negatively charged sulfur interstitial, respectively. In addition, the divalence state of sulfur atoms for the material is evidenced by XPS S-2p spectra in Fig. S3).

Compared to the sample before test 1, the EPR signal at g = 2.003 gradually increases for the sample after photocatalytic test (after test 1) and for the sample with subsequent standing (before test 2). This suggests that a part of the sulfur vacancies are in-situ created during the photocatalytic and standing (light off) process. However, EPR is a very sensitive technique for detecting defects that possess unpaired electrons. The increment of the EPR signals ranging from ~0.1–0.2 (scale bar) corresponds to low concentration of vacancies [34], which may not solely contribute to the dramatically enhanced activity for H_2 production. The low concentration of the sulfur vacancies and sulfur interstitials are also supported from the similar UV–vis spectra for all three samples. Comparing the sample before test 1, only slightly increased light absorption in visible region for the sample before test 2 is found (Fig. S4).

Alternative reasonable interpretation is that the in-situ rearrangement of the randomly distributed sulfur vacancies and sulfur interstitials within the material may synergistically contribute to the

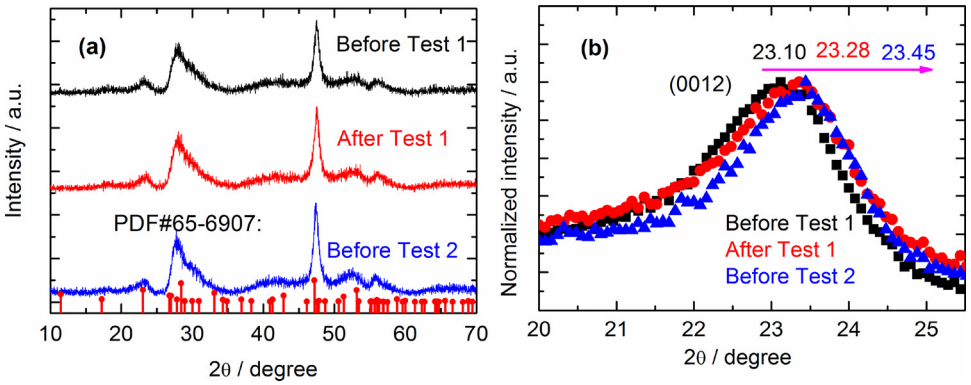

Fig. 4. **(a)** XRD patterns of the defective $Zn_2In_2S_5$ nanosheets before test 1, after test 1 and before test 2 (Red dot-lines represent standard data (PDF No. 65-6907) of rhombohedral $Zn_2In_2S_5$). **(b)** Slow scan of the XRD peak at lattice plane of (0012) (For interpretation of the references to colour in this figure legend, the reader is referred to the web version of this article).

dramatically enhanced activity for H_2 production. The rearrangement of the sulfur vacancies and sulfur interstitials are supported by the high resolution TEM images of the sample before test 2 (Fig. S5) that the disconnected lattice fringes are much more ordered than that of the sample before test 1 (Fig. 1b).

The rearrangement of the randomly distributed sulfur vacancies and sulfur interstitials is further supported by XRD patterns. As indicated in Fig. 4a, XRD patterns of all samples before and after photocatalytic tests well match with standard data of rhombohedral $Zn_2In_2S_5$ (PDF No. 65-6907, a = 3.85 Å, c = 46.27 Å), which has an atomic layer structure arranged in a repeated sequence of S-Zn-S-In-S-Zn-S-In-S along the *c*-axis. No impurity phases could be identified. This is in accordance with XPS survey spectra that no external dopants are introduced for the sample before and after photocatalytic tests. As indicated in Fig. 4b, slow scan to the single peak at (0012) gives obvious peak shift from 23.1° for the sample before test 1 to obviously larger values at 23.28 and 23.45° for the samples after test 1 and before test 2, respectively. This means significant shrinkage of lattice spacing both in photocatalytic and standing (light off) process. Although it is widely accepted that vacancies could slightly reduce the crystal lattice spacing [35], the sulfur interstitials should more or less expand the lattice [36]. The obvious peak shift (0.3°) should not be attributed to increase of sulfur vacancies, due to counteract effect of the same amount of interstitial atoms. Alternative route is that the sulfur vacancies and sulfur interstitials are rearranged during photocatalytic and standing process. The Coulomb attraction between the positively charged sulfur vacancies and negatively charge sulfur interstitials could easily form stable vacancy-interstitial defect associates during the rearrangement [37]. The attraction between the positively charged vacancies and negatively charged interstitials could tighten the atoms nearby during the structure rearrangement, which results in obviously reduced lattice spacing at (0012).

Based on the analysis above, the following mechanism is proposed step by step that the randomly distributed sulfur vacancies and sulfur interstitials within the synthesized material are in-situ properly rearranged to form defect associates. The properly rearranged sulfur vacancies and sulfur interstitials synergistically promote the photocatalytic water splitting for H_2 production.

(1) Creation of sulfur vacancies

$$S_s^x \xrightarrow{Zn_2In_2S_5} V_s^{\bullet\bullet} + S_i^{//} \quad (1)$$

$$S_s^x(surface) + H_2O \xrightarrow{Zn_2In_2S_5} V_s^{\bullet\bullet} + HS^- + OH^- \quad (2)$$

As discussed before, the dislocation of the lattice sulfur atoms in layered structure would automatically result in positively charged sulfur vacancies and negatively charged sulfur interstitials (reaction (1)). Dislocation of the lattice sulfurs to form sulfur vacancies and sulfur interstitials is supported from EPR and PL spectra that sulfur interstitials and sulfur vacancies simultaneously increase after photocatalytic process. These defects naturally coexist within the synthesized material. However, these defects are randomly distributed in the crystal structure, which are supported from irregularly disconnected TEM fringes. In addition, the contact of the material surface with H_2O would also be expected to generate a certain amount of sulfur vacancies (reaction (2)). This is supported from the EPR results that the concentration of sulfur vacancies also increases during standing (light off) process.

(2) Trapping of O atoms at sulfur vacancy sites

$$Na_2S \rightarrow 2Na^+ + S^{2-} \quad (3)$$

$$S^{2-} + H_2O \rightarrow HS^- + OH^- \quad (4)$$

$$OH^- + V_S^{\bullet\bullet} \xrightarrow{k_1} O_S + H^+ \quad (5)$$

When Na_2S is dissolved into the aqueous solution, it will be quickly transformed into Na^+ and S^{2-} ions (reaction (3)). The S^{2-} ions would be further fully converted to more negatively charged OH^- and less negatively charged HS– in aqueous solution [38], as indicated in reaction (4). The negatively charged OH– groups are more likely to be attracted by positively charged sulfur vacancy sites than that of the HS– groups, accompanied with trapping of O atoms in sulfur vacancy sites (Fig. 5). The trapping of the O atoms at sulfur vacancy sites would reduce the O—H bond energy. This would facilitate the release of protons (H^+), as indicated in reaction (5).

(3) Removing trapped O atoms to reactivate sulfur vacancies

$$3O_S^x + HS^- \rightarrow SO_3^{2-} + 3V_S + H^+ / 4O_S^x + HS^- \rightarrow SO_4^{2-} + 4V_S + H^+ \quad (6)$$

$$h\nu \xrightarrow{Zn_2In_2S_5} e^- + h^+ \quad (7)$$

$$2H^+ + 2e^/ \rightarrow H_2(gas) \quad (8)$$

$$V_S + 2h^+ \rightarrow V_S^{\bullet\bullet} \quad (9)$$

However, the trapped O atoms at sulfur vacancy sites are not well matching, are therefore chemically not stable. Due to high reducibility of HS– ions, the trapped O atoms tend to react with the HS– ions to form neutral sulfur vacancies (V_s) and SO_3^{2-}/SO_4^{2-} groups (mixture of SO_3^{2-} and SO_4^{2-} groups is supported from Fig. S6), which is accompanied with releasing protons (reaction (6)). The released protons from reactions (5) and (6) are easily converted to H_2 upon capturing photo-generated electrons (reactions (7) and (8)). In contrast, the neutral sulfur vacancies tend to combine with photo-generated holes to form positively charged sulfur vacancies again (reaction (9)). This means the reactivation of the sulfur vacancies through removing O atoms at vacancy sites using HS– ions, which originate from Na_2S sacrificial reagent.

The proposed Na_2S sacrificial reagent for reactivating sulfur vacancies is supported by comparing the catalytic performance of the sample with and without Na_2S (Fig. 6a). Without Na_2S, the sample exhibits much less H_2 production rate at the second cycle test than that

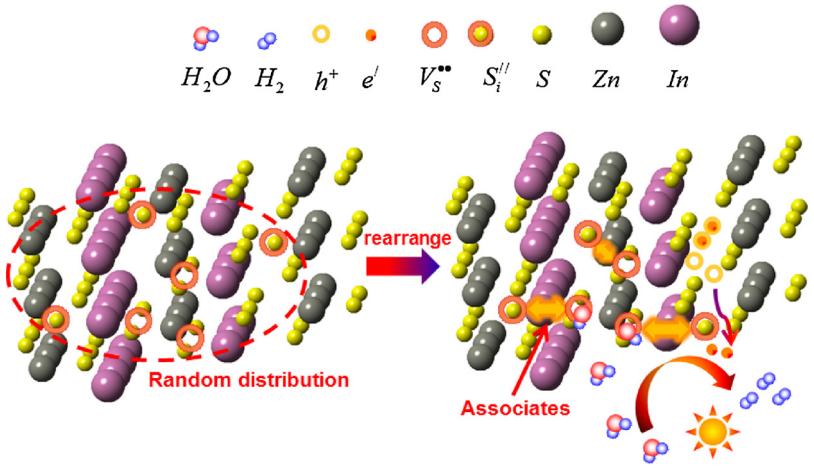

Fig. 5. Scheme of the synergistic effect of the rearranged sulfur vacancies and sulfur interstitials for improving charge-carrier separation and promoting photocatalytic water splitting into H_2 via trapping O atoms into sulfur vacancy sites.

of the first cycle, which means serious deactivation. This is due to the continuously trapped O atoms at the sulfur vacancy sites, which cannot be removed if no Na_2S is added. Thus, the serious deactivation occurs. In contrast, with Na_2S, the sample exhibits much more H_2 production rate at the second cycle test than that of the first cycle test. This suggests that the sulfur vacancies are very important species for improving the catalytic performance.

(4) Formation of defect associates

$$V_S^{\bullet\bullet} + S_i^{//} \rightarrow V_S^{\bullet\bullet} - S_i^{//} \quad (10)$$

Due to the Coulomb attraction and mobility of vacancy defects [39,40], the positively charged sulfur vacancies are likely to diffuse closer to negatively charged interstitials to form thermodynamically more stable defect associates (reaction (10)) with increase of time during catalytic and standing process. Alternatively, the positively charged vacancies and negatively charged interstitials are also possible to recombine to form much more stable lattice sulfurs during the rearrangement. However, this is contradictory to what is observed from EPR spectra. The stable co-existence of the sulfur vacancies and sulfur interstitials could be due to the layered structure of rhombohedral $Zn_2In_2S_5$ possessing massive space between atomic layers [41], which could easily accommodate the interstitial atoms. Furthermore, the relatively large metal atoms between sulfur vacancies and sulfur interstitials could prevent the possible recombination of the defects (Fig. 5). Formation of the defect associates are further supported by XPS S-2p spectra. As sulfur atoms are directly connected to Zn and In atoms to form Zn-S and In-S chemical bonds, the formation of sulfur defect associates should reduce the bonding energy of sulfur atoms on average. This is supported from Fig. S3 that the binding energy of S-2p obviously shifts to lower values from 161.52 eV (before test 1) to 161.35 eV (before test 2).

The contribution of the sulfur defect associates for separating photo-generated charge-carriers is investigated by transient photocurrent spectra, which directly reflect the ability to generate and transfer photo-generated charge-carriers [42]. Notably, the sample before test 2 exhibits much more (~2-fold) photocurrent density under visible light irradiation than that of the sample before test 1 (Fig. 6b). This demonstrates that the formation of sulfur defect associates can actually improve the photo-generated charge-carrier separation. A reasonable explanation is that the properly rearranged positively charged sulfur vacancies and negatively charged sulfur interstitials form internal electric filed that efficiently separate the photo-generated electron and holes. In addition, the photocurrent performances are similar for the four continuous on-off cycles. This suggests that the defect associates are stably present without recombination to form lattice sulfurs, which is well in accordance with our EPR and XRD results.

The synergetic contribution of the sulfur vacancies and sulfur interstitials for dramatically enhanced photocatalytic H_2 production is further supported by continuous third and fourth cycle tests (Test 3 and Test 4 in Fig. 7a). Again, the H_2 production rates obviously increase for Test 3 and Test 4 comparing to that of the Test 1 and Test 2. The H_2 production rate at the end of the fourth cycle (Test 4) is 511 μmol/g/h, and is stabilized at the fifth and sixth tests (Test 5 and Test 6), which is 13-fold more than that of the first hour of first cycle (Test 1) in Fig. 2. The photocatalytic results well corresponds to EPR results in Fig. S7 that the sulfur vacancies (g = 2.003) of the sample before test 4 is higher than that of the sample before test 2, and the sample before test 5 shows almost the same intensity of EPR signal comparing to that of

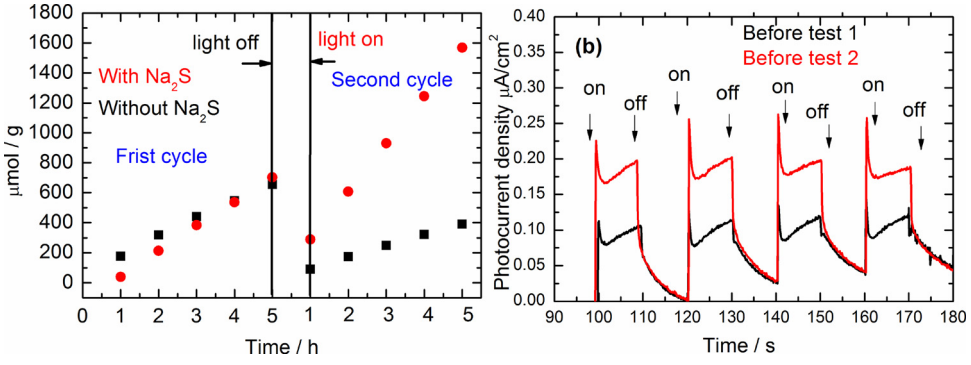

Fig. 6. (a) Photocatalytic cycle tests of defective $Zn_2In_2S_5$ nanosheets for splitting water into H_2 with and without Na_2S sacrificial reagent. **(b)** Transient photocurrent responses of the defective $Zn_2In_2S_5$ nanosheets during visible light on/off cycles.

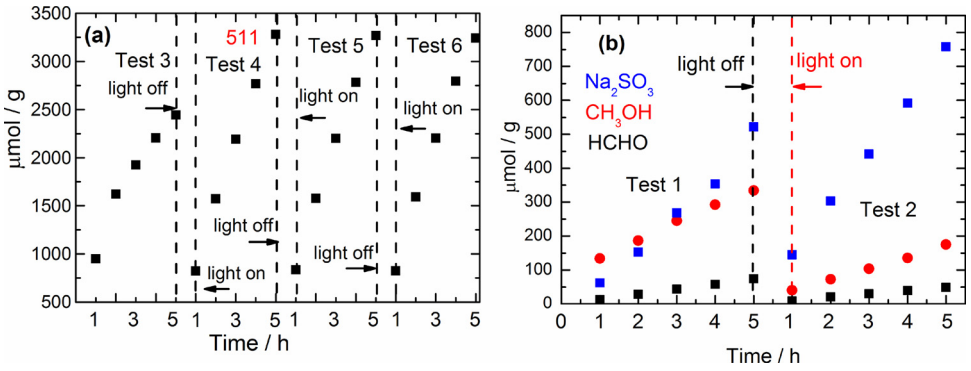

Fig. 7. **(a)** Photocatalytic cycle tests (Test 3 to Test 6) of defective $Zn_2In_2S_5$ nanosheets under visible light irradiation using Na_2S as sacrificial reagent. **(b)** With different sacrificial reagents (Na_2SO_3, CH_3OH, HCHO).

the sample before test 4, which means stabilization of the defects within the material. This further confirms our analysis that sulfur vacancies positively contribute to the photocatalytic H_2 production.

Further comparison of Fig. 6b with Fig. 7a indicates that ~2-fold enhanced photocurrent density cannot well explain the 13-fold enhanced activity for H_2 production. The dramatically increased H_2 production rate firmly supports the proposal that sulfur interstitials and sulfur vacancies synergistically contribute to the dramatically increased activity for H_2 production.

The proposed mechanism is further explored using different sacrificial reagents for photocatalytic splitting water into H_2. As commonly reported for sulfur based materials [43,44], the serious de-activation occurs when HCHO and CH_3OH are used as sacrificial reagents (Fig. 7b). This means that both HCHO and CH_3OH are not reactive enough to remove the trapped O atoms from sulfur vacancy sites. In contrast, the promoted photocatalytic performance with irradiation from Test 1 to Test 2 is also observed for the sample using Na_2SO_3 as sacrificial reagent. However, the activity is not yet comparable to that of the sample with Na_2S. Further exploration using more active sacrificial reagents to efficiently remove O atoms at sulfur vacancy sites could further optimize the catalytic performance.

4. Conclusions

In conclusion, a new strategy is proposed to significantly improve the photocatalytic performance, which is based on the synergistic effect of the rearranged sulfur vacancies and sulfur interstitials in $Zn_2In_2S_5$ without introducing any external dopants. Toward this, the defective $Zn_2In_2S_5$ nanosheets have been successfully synthesized by a simple hydrothermal method. The rearranged sulfur vacancies and sulfur interstitials obviously (~2-fold) enhance the photo-generated charge-carrier separation efficiency, and dramatically promote the photocatalytic water splitting for H_2 production. The promoted catalytic performance is supported by that the H_2 production rate at the end of the fourth cycle is 13-fold more than that of the beginning of the first cycle test. However, the 2-fold enhanced charge-carrier separation efficiency cannot explain the 13-fold enhanced activity. Therefore, the 13-fold enhanced activity for H_2 production should be attributed to a synergistic effect: the electric filed formed from the defect associates effectively separate the photo-generated charge-carriers, and sulfur vacancies act as active sites for continuously trapping O atoms of OH– groups (originated from H_2O) to produce H^+ ions, which would be easily converted to H_2 upon capturing the photo-generated electrons. The new strategy based on synergistic effect of the oppositely charged intrinsic defects for sharply enhanced photocatalytic performance without assistance of external dopants could also apply to other metal sulfur material systems, e.g., CdS, ZnS, $CuInS_2$. This strategy could also be widely extended for application of other defects (e.g., oxygen vacancies, oxygen interstitials, zinc vacancies, zinc interstitials) in other semiconductor material systems.

Acknowledgements

This work is supportedby the National Natural Science Foundation of China (21673242, 11674318, 51472242), the Project of State Key Laboratory of Structural Chemistry (20170015) and the Fujian Provincial Orienting Sci & Tech Project (2016H0046).

Appendix A. Supplementary data

Supplementary material related to this article can be found, in the online version, at doi:https://doi.org/10.1016/j.apcatb.2018.09.008.

References

[1] X. Chen, S. Shen, L. Guo, S.S. Mao, Chem. Rev. 110 (2010) 6503–6570.
[2] M. Ni, M.K.H. Leung, D.Y.C. Leung, K.A. Sumathy, Renew. Sust. Energy Rev. 11 (2007) 401–425.
[3] Y. Xu, Y. Huang, B. Zhang, Inorg. Chem. Front. 3 (2016) 591–615.
[4] M.D. Kärkäs, O. Verho, E.V. Johnston, B. Åkermark, Chem. Rev. 114 (2014) 11863–12001.
[5] Z. Zhang, L. Huang, J. Zhang, F. Wang, Y. Xie, X. Shang, Y. Gu, H. Zhao, X. Wang, Appl. Catal. B: Environ. 233 (2018) 112–119.
[6] A. Mills, S.L. Hunte, J. Photochem. Photobiol. A 108 (1997) 1–35.
[7] M.R. Hoffmann, S.T. Martin, W. Choi, D.W. Bahnemann, Chem. Rev. 95 (1995) 69–96.
[8] H. Tong, S. Ouyang, Y. Bi, N. Umezawa, M. Oshikiri, J. Ye, Adv. Mater. 24 (2012) 229–251.
[9] A.M. Smith, S. Nie, Acc. Chem. Res. 43 (2010) 190–200.
[10] G. Ye, Y. Gong, J. Lin, B. Li, Y. He, S.T. Pantelides, W. Zhou, R. Vajtai, P.M. Ajayan, Nano Lett. 16 (2016) 1097–1103.
[11] Q. Sun, D. Cortie, S. Zhang, T.J. Frankcombe, G. She, J. Gao, L.R. Sheppard, W. Hu, H. Chen, S. Zhuo, D. Chen, R.L. Withers, G. Mclntyre, D. Yu, W. Shi, Y. Liu, Adv. Mater. 29 (2017) 1605123.
[12] X. Zhang, Z. Zhao, W. Zhang, G. Zhang, D. Qu, X. Miao, S. Sun, Z. Sun, Small 12 (2016) 793–801.
[13] S. Shen, L. Zhao, L. Guo, Int. J. Hydrogen Energy 35 (2010) 10148–10154.
[14] Z. Lei, W. You, M. Liu, G. Zhou, T. Takata, M. Hara, K. Domen, C. Li, Chem. Comm. 17 (2003) 2142–2143.
[15] X. Jiao, Z. Chen, X. Li, Y. Sun, S. Gao, W. Yan, C. Wang, Q. Zhang, Y. Lin, Y. Luo, Y. Xie, J. Am. Chem. Soc. 139 (2017) 7586–7594.
[16] Y. Liu, Y. Xie, L. Liu, J. Jiao, Catal. Sci. Technol. 7 (2017) 5635–5643.
[17] Z.G. Yu, Y. Zhang, B.I. Yakobson, Nano Lett. 15 (2015) 6855–6861.
[18] K.W. Böer, W.J. Nalesnik, Mater. Res. Bull. 4 (1969) 153–160.
[19] A. Polizzotti, A. Faghaninia, J.R. Poindexter, L. Nienhaus, V. Steinmann, R.L.Z. Hoye, A. Felten, A. Deynine, N.M. Mangan, J.P. Correa-Baena, S.S. Shin, S. Jaffer, M.G. Bawendi, C. Lo, T. Buonassisi, J. Phys. Chem. Lett. 8 (2017) 3661–3667.
[20] F. Tian, R. Zhu, K. Song, M. Niu, F. Ouyang, G. Cao, Mater. Res. Bull. 70 (2015) 645–650.
[21] J. Chen, X. Wu, L. Yin, B. Li, X. Hong, Z. Fan, B. Chen, C. Xue, H. Zhang, Angew. Chem. 126 (2014) 1–6.
[22] S. Zhang, X. Liu, C. Liu, S. Luo, L. Wang, T. Cai, Y. Zeng, J. Yuan, W. Dong, Y. Pei, Y. Liu, ACS Nano 12 (2018) 751–758.
[23] M. Guan, C. Xiao, J. Zhang, S. Fan, R. An, Q. Cheng, J. Xie, M. Zhou, B. Ye, Y. Xie, J. Am. Chem. Soc. 135 (2013) 10411–10417.
[24] W. Yang, B. Liu, T. Fang, W. Jennifer, L. Christophe, Z. Li, X. Zhang, X. Jiang, Nanoscale 8 (2016) 18197–18203.

[25] W. Yang, L. Zhang, J. Xie, X. Zhang, Q. Liu, T. Yao, S. Wei, Q. Zhang, Y. Xie, Angew. Chem. 128 (2016) 6828–6832.
[26] M. Kong, Y. Li, X. Chen, T. Tian, P. Fang, F. Zheng, X. Zhao, J. Am. Chem. Soc. 133 (2011) 16414–16417.
[27] S.I. Radautsan, F.G. Donika, G.A. Kyosse, I.G. Mustya, V.F. Zhitar, Phys. Status Solidi 34 (1969) 129–131.
[28] J. Xie, J. Zhang, S. Li, F. Grote, X. Zhang, H. Zhang, R. Wang, Y. Lei, B. Pan, Y. Xie, J. Am. Chem. Soc. 135 (2013) 17881–17888.
[29] R.R. Chianelli, M.J. Ledoux, Adv. Catal. 40 (1994) 177–232.
[30] Z. Fang, S. Weng, X. Ye, W. Feng, Z. Zheng, M. Lu, S. Lin, X. Fu, P. Liu, ACS Appl. Mater. Interfaces 7 (2015) 13915–13924.
[31] D. Denzler, M. Olschewski, K. Sattler, J. Appl. Phys. 84 (1998) 2841–2845.
[32] W. Zhou, X. Zou, S. Najmaei, Z. Liu, Y. Shi, J. Kong, J. Lou, P.M. Ajayan, B.I. Yakobson, J. Idrobo, Nano Lett. 13 (2013) 2615–2622.
[33] Y.M. Chiang, D.P. Birnie, W.D. Kingery, Physical Ceramics, Wiley, New York, 1997.
[34] D.E. Motaung, P.R. Makgwane, S.S. Ray, Mater. Lett. 139 (2015) 475–479.
[35] Q. Wu, Q. Zheng, R. Van de Krol, J. Phys. Chem. C 116 (2012) 7219–7226.
[36] D. Bai, J. Zhang, Z. Jin, H. Bian, K. Wang, H. Wang, L. Liang, Q. Wang, S.F. Liu, ACS Energy Lett. 3 (2018) 970–978.
[37] V. Kumar, F.A. Kröger, J. Solid State Chem. 3 (1971) 387–400.
[38] V. Chakrapani, D. Baker, P.V. Kamat, J. Am. Chem. Soc. 133 (2011) 9607–9615.
[39] Q. Wu, R. Van de Krol, J. Am. Chem. Soc. 134 (2012) 9369–9375.
[40] R. Schaub, E. Wahlström, A. Rønnau, E. Lægsgaard, I. Stensgaard, F. Besenbacher, Science 299 (2003) 377–379.
[41] Z. Xu, Y. Li, S. Peng, G. Lu, S. Li, CrystEngComm 12 (2011) 4770–4776.
[42] Q. Xiang, J. Yu, M. Jaroniec, J. Phys. Chem. C 115 (2011) 7355–7363.
[43] C. Liao, C. Huang, J.C.S. Wu, Catalysts 2 (2012) 490–516.
[44] N. Bao, L. Shen, T. Takata, K. Domen, Chem. Mater. 20 (2008) 110–117.